CHAPTER
FOUR

The Detailed Model

In order to optimize the shell and coil heat exchanger design using the model presented in Chapter 3, one would have to build several heat exchanger prototypes, and then run tests on them in order to produce the required shear pressure drop and modified effectiveness curves. This could prove to be an expensive and time consuming process. The use of the detailed model, presented in this chapter, simplifies the design of an optimal shell and coil natural convection heat exchanger. The detailed model is based upon empirical crossflow correlations found in heat transfer texts rather than experimental pressure drop and modified effectiveness curves. (A model for concentric tube counterflow heat exchangers is presented in Appendix A). The detailed model is applicable solely to shell and coil heat exchangers. By varying the geometry of the heat exchanger in the model, the detailed model can be used as a tool towards the optimization of the design of a shell and coil NCHE. As the only difference between the detailed and the simple model lies in the NCHE shear pressure drop and heat transfer analyses, this chapter (and Appendix A) will present only those aspects of the detailed model which deviate from the simple model.

4.1 Geometry of a Shell and Coil NCHE

As there currently are no pressure drop or heat transfer correlations for forced flow over helical coils, correlations are used instead for bundles of tubes in crossflow. The first step therefore, is the modification of the geometry of the coils such that they can be represented as bundles of tubes.

4.1.1 Transforming Concentric Helices into an Equivalent Tube Bundle

For every pitch length, one complete revolution of each coil is exposed to crossflow. Hence if the slope of the tubes are neglected, the coils have nearly the same pressure drop as would a series of toroids of the same diameter. Consider Figure 4.1.1. As a first step in altering the coil geometry, the coils are cut at one position along the perimeter giving a series of toroids, as shown in Figure 4.1.2.

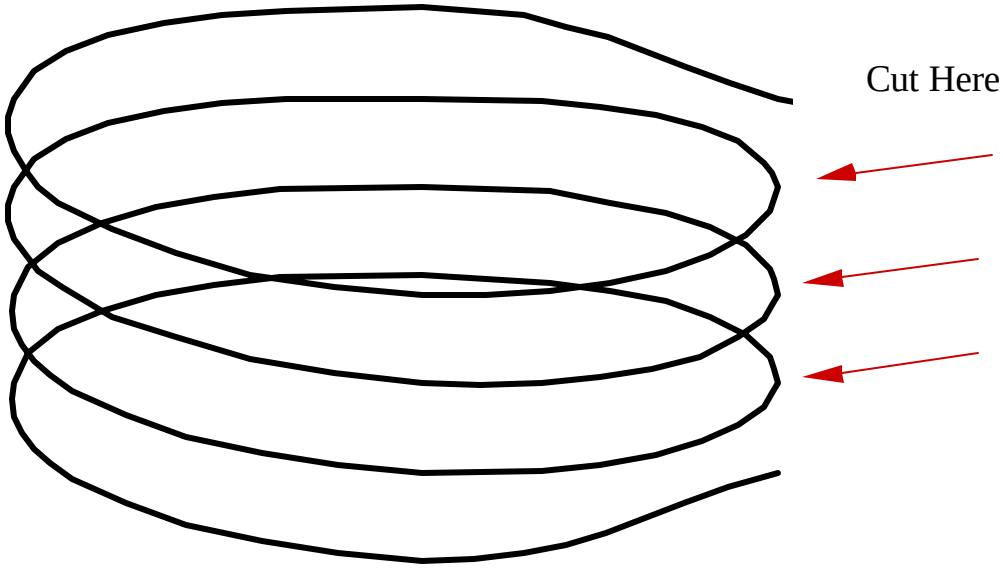

Figure 4.1.1 Cutting a coil to transform it into toroids.

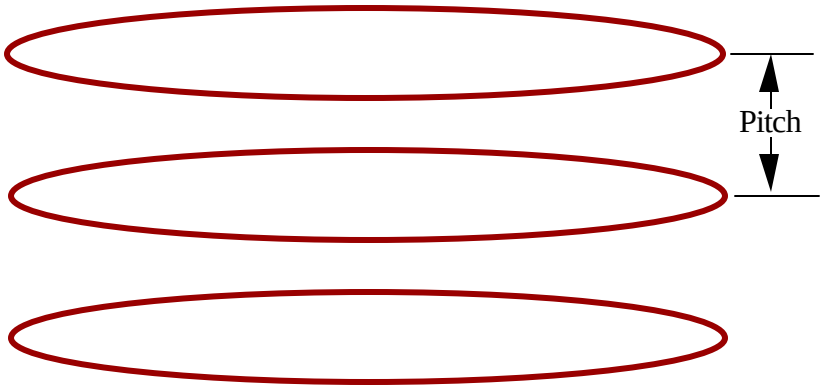

Figure 4.1.2 A coil transformed into a column of toroids.

As shown in Figure 4.1.3, these toroids are then cut and stretched out, so as to resemble straight tubes in crossflow. As there are four coils, each within the other, there now will be four columns of straight tubes, each of different length.

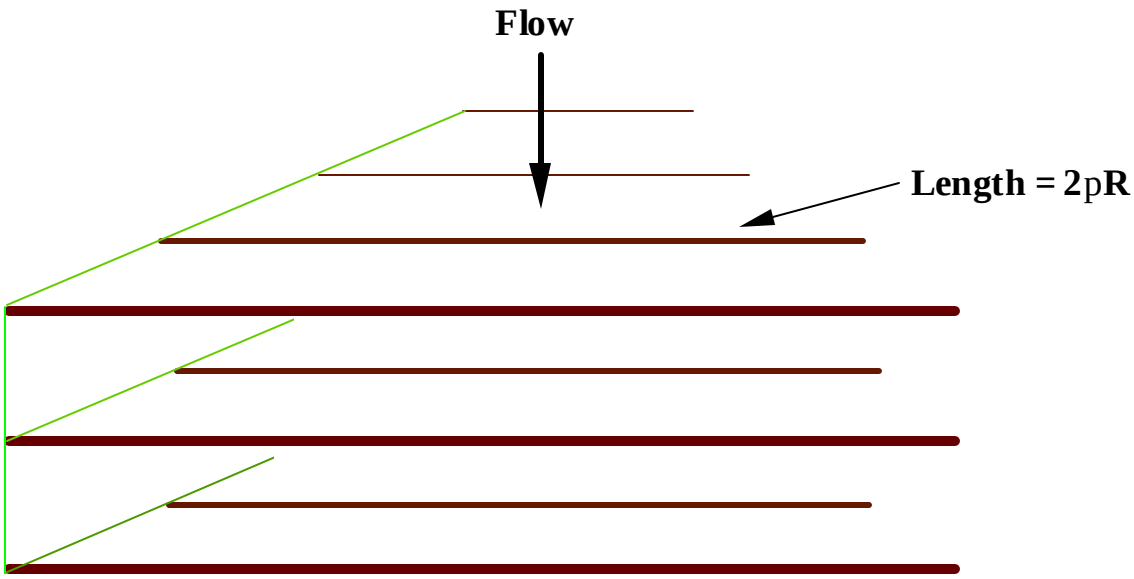

Figure 4.1.3 Toroids cut and straightened.

An average of these lengths is taken so that the bundle of tubes now can be represented as a bundle of tubes in crossflow, like that for which heat transfer and pressure drop correlations are available. Figure 4.1.4 depicts the transformed coils as a bundle of tubes in crossflow.

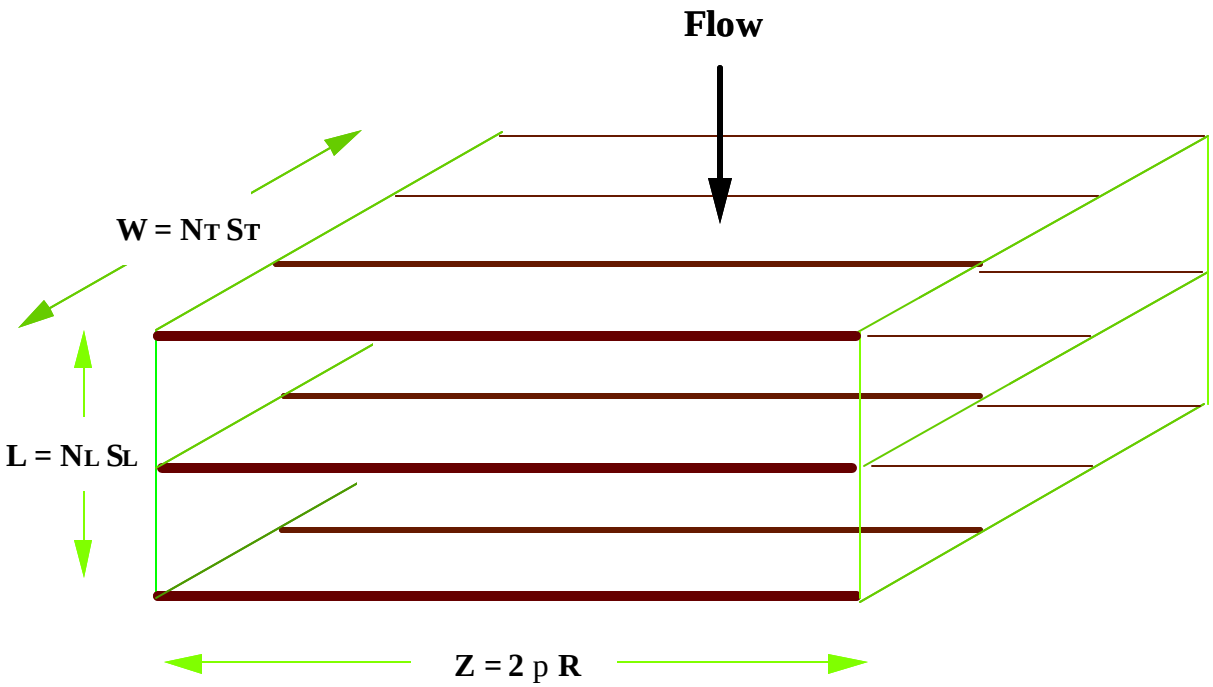

Figure 4.1.4 Equivalent bundle of tubes in crossflow extracted from four concentric helical coils.

4.1.2 Geometry of Tubes in Crossflow

The coil pitch becomes S_L, while S_T is measured as the average distance between the coils in the transverse direction, as is shown in Figure 4.1.5.

The number of tube rows in the longitudinal direction is found using:

$$N_L = \frac{H}{S_L} \tag{4.1.1}$$

where H represents the height of the heat exchanger.

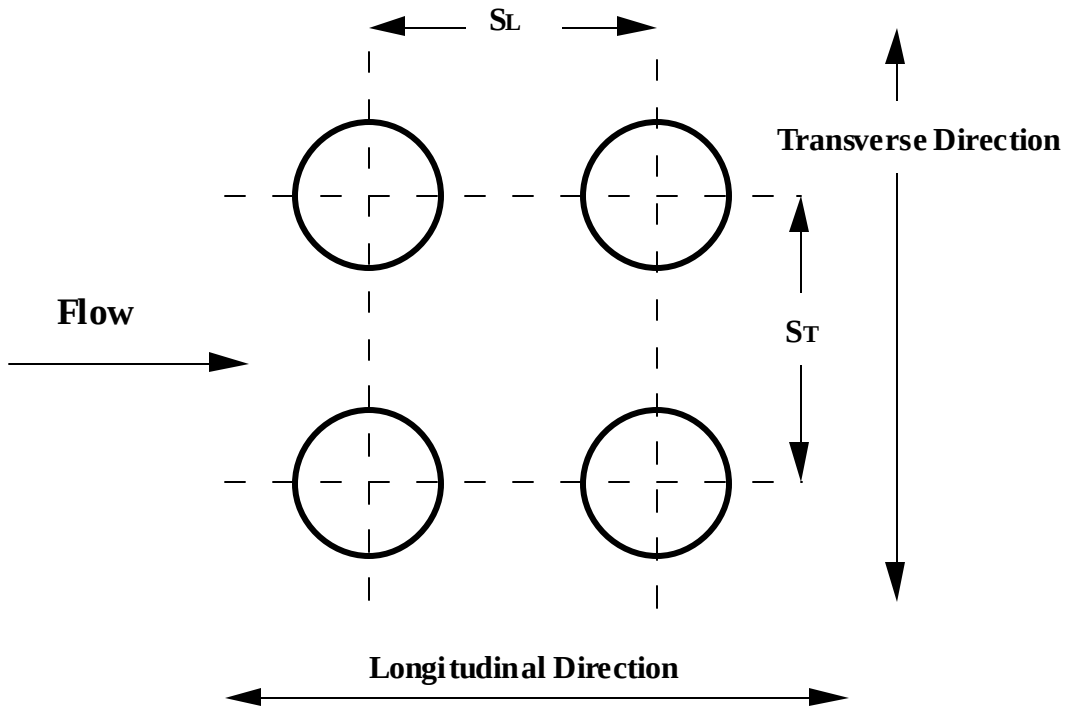

Figure 4.1.5 Determination of S_L and S_T.

There are four columns of tubes wide, one for each coil, hence,

$$N_T = 4 \tag{4.1.2}$$

The depth, Z, is found by averaging the lengths of the tubes:

$$Z = \frac{\sum_{i}^{N_{coils}} p\, D_c}{N_T} \tag{4.1.3}$$

where D_c is the coil diameter.

The tube outer surface area is found using:

$$A_{s,o} = \pi\, D_{t,o}\, Z\, N \tag{4.1.4}$$

where $D_{t,o}$ is the tube outer diameter and N is the total number of tubes.

4.1.3 Yaw Angle

The yaw angle is the angle at which the flow meets the tubes, which is detailed in Figure 4.1.6. Normally in crossflow, the yaw angle is 90°. Experiments have been done relating pressure drops and heat transfer to the yaw angle on tubes in crossflow. This will be discussed in Section 4.2.3. As the tubes in the coils originally were slanted (i.e. with a yaw angle < 90°) , the tube bundle derivative should be considered slanted as well.

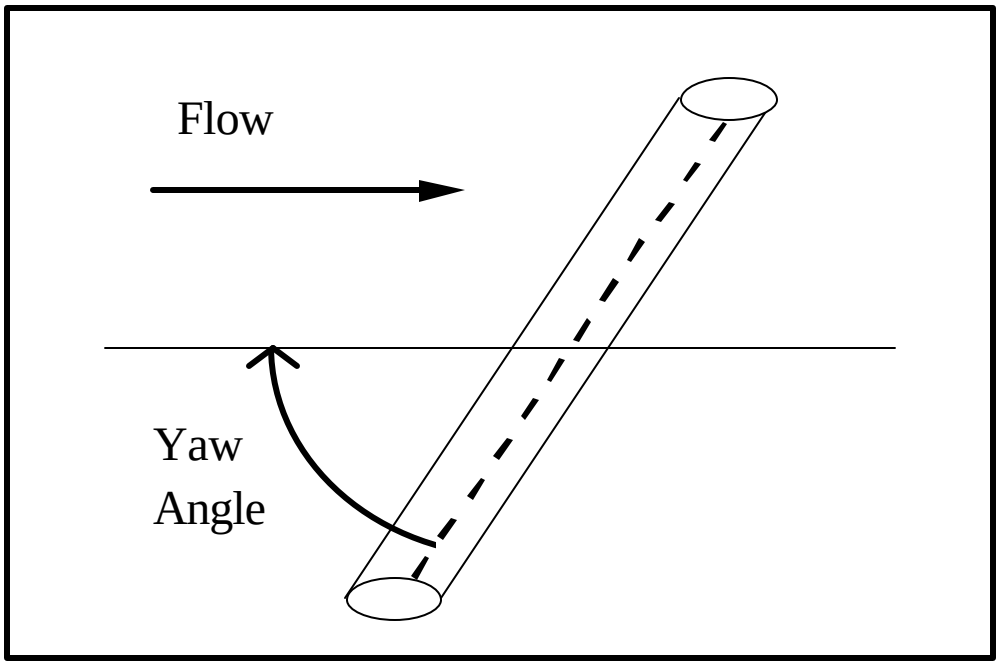

Figure 4.1.6 Yaw Angle.

Each yaw angle is found using simple trigonometry:

$$\beta_i = \tan^{-1}\left(\frac{\frac{1}{2}pitch}{D_c}\right) \qquad (4.1.5)$$

where D_c is the diameter of the respective coil. The yaw angles are then averaged to find a mean yaw angle.

4.2 Detailed Model Pressure Drop Calculation

In a natural convection system, it is important to get an accurate accounting for pressure drop, as pressure differences are what determine the water flow rate.

4.2.1 Minor Losses

The minor losses associated with the Thermo Dynamics' NCHE are 45° and 90° ells, and pipe entrance and exit conditions. These are shown in Figure 4.2.1.

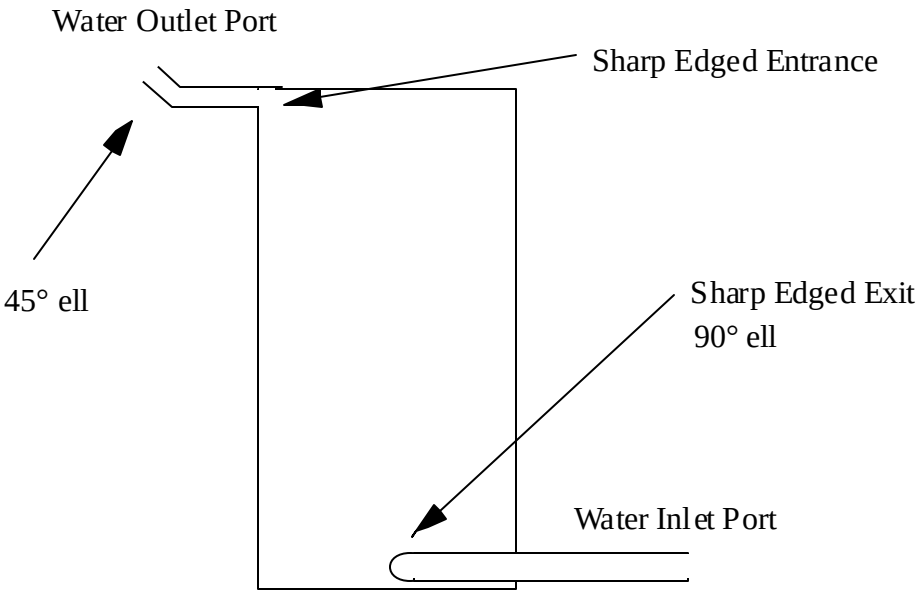

Figure 4.2.1 Minor losses associated with Thermo Dynamics' NCHE.

In the analysis of the NCHE, the calculation of the minor losses is important. Figure 4.2.2 shows that the minor losses account for the bulk of the heat exchanger pressure loss.

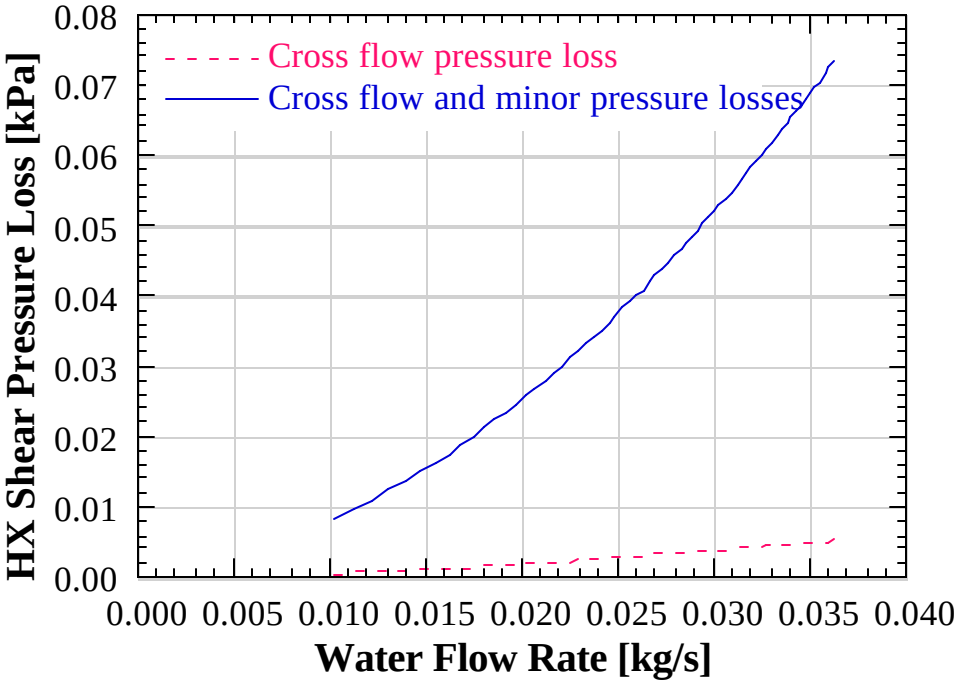

Figure 4.2.2 Comparison of minor and major losses in NCHE.

Tables with listings of minor losses attributable to pipe fittings assume fully developed turbulent flow. In a natural convection system, flow will generally remain laminar, hence the minor loss coefficients provided by tables will not be accurate for this application. Many tables also have little regard for pipe fitting size. Hooper's correlation provides minor loss coefficients for both laminar and turbulent flow in pipes (Kakic 1987). In this analysis, Hooper's correlation was used for the 45° and 90° pipe bends:

$$K^* = K_1 Re^{-1} + K_\infty \left(1 + 0.5\, a^*\right) \qquad (4.2.1)$$

where a^* = fitting radius in inches ,

$K_1 = K^*$ at $Re = 1$,

$K_\infty = K^*$ at $Re = \infty$.

Hooper provides a chart with listings of different fittings and their respective K_1 and K_8 values. An explanation of R and a is provided in Figure 4.2.3.

Table 4.2.1 Hooper's Correlation *K* Constants

Bend	Fitting Radius	R/a	Type	K_1	K_8
90	standard	2	screwed	800	0.40
90	standard	2	flanged, welded	800	0.25
90	long radius	3	all types	800	0.20
45	standard	2	all types	500	0.20
45	long radius	3	all types	500	0.15

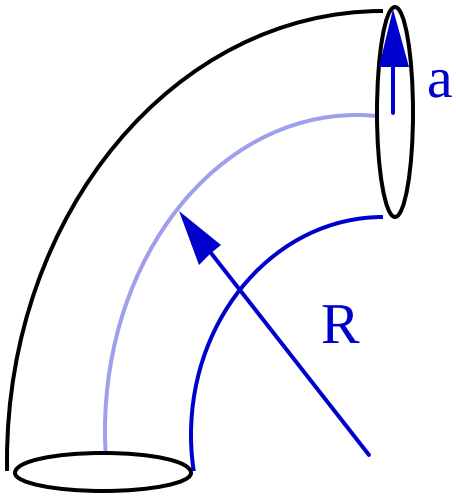

Figure 4.2.3 R and a values for pipe ells

Figure 4.2.4 compares the calculated shear pressure losses found for the two ells using table values for minor losses and Hooper's correlation. As will be shown, the pressure loss difference shown for the 90° ell is sufficient to significantly alter the shear pressure drop analysis.

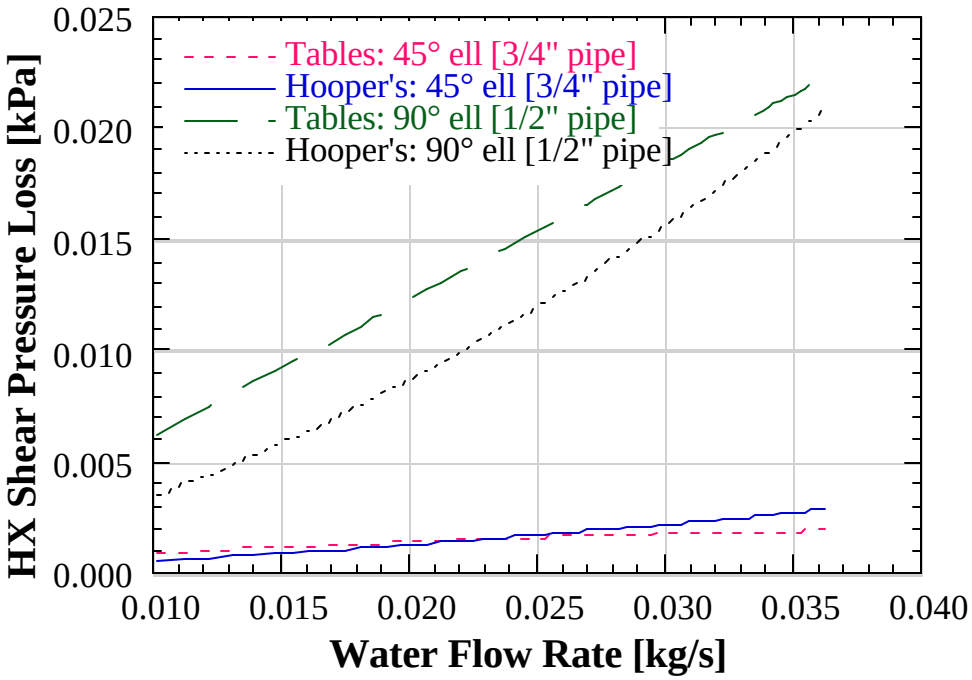

Figure 4.2.4 Comparison of table values and Hooper's correlation for shear pressure loss in NCHE ells.

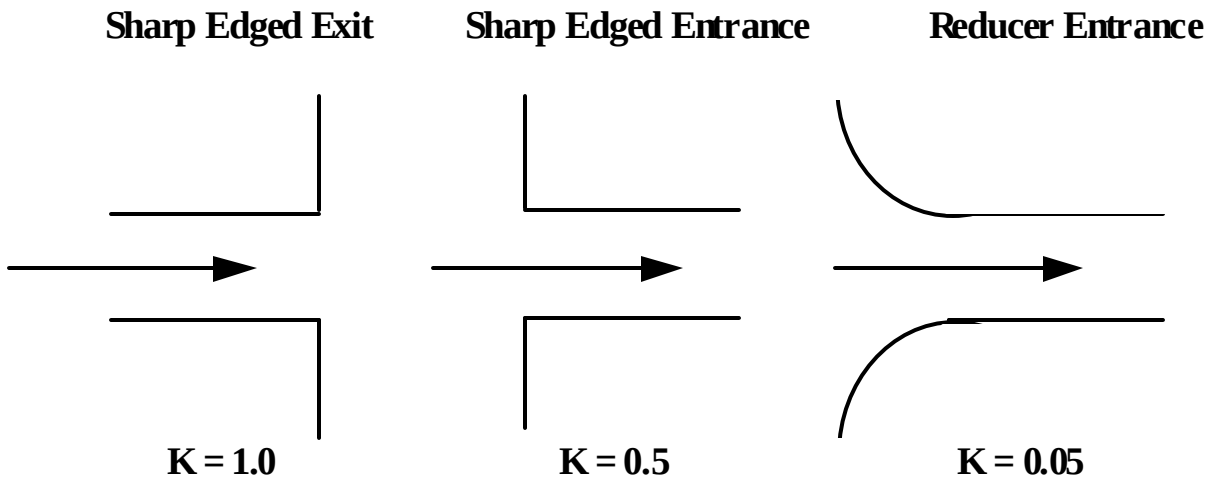

Figure 4.2.5 Entrance and exit minor loss K values found in tables. Minor loss coefficient tables assume turbulent flow.

No correlations or laminar table values were found for flow entrance and flow exit configurations. Flow exits are generally assigned a minor loss coefficient of K=1.0. Sharp edged entrances are assigned K=0.50, and for reducer inlets, K can be as little as 0.05, as is shown in Figure 4.2.5 (Cheremisinoff, 1981).

Technicians at Thermo Dynamics were asked about the entrance condition, whether it was sharp-edged or smooth as is shown in Figure 3.2.5. The entrance was just simply attached. Smoothing the entrance would be too difficult and costly a task. Still it was somewhat smooth. For this reason, the minor loss coefficient assigned to the entrance was K=0.4.

The minor loss coefficients were translated into effective lengths using:

$$L_e = \frac{K \dot{m} Y}{16 \pi \mu} \tag{3.2.8}$$

The minor losses associated with their respective fittings was then found from:

$$\Delta P_{sh} = f_D \frac{L_e}{D_p} \rho \frac{V^2}{2} \tag{3.2.7}$$

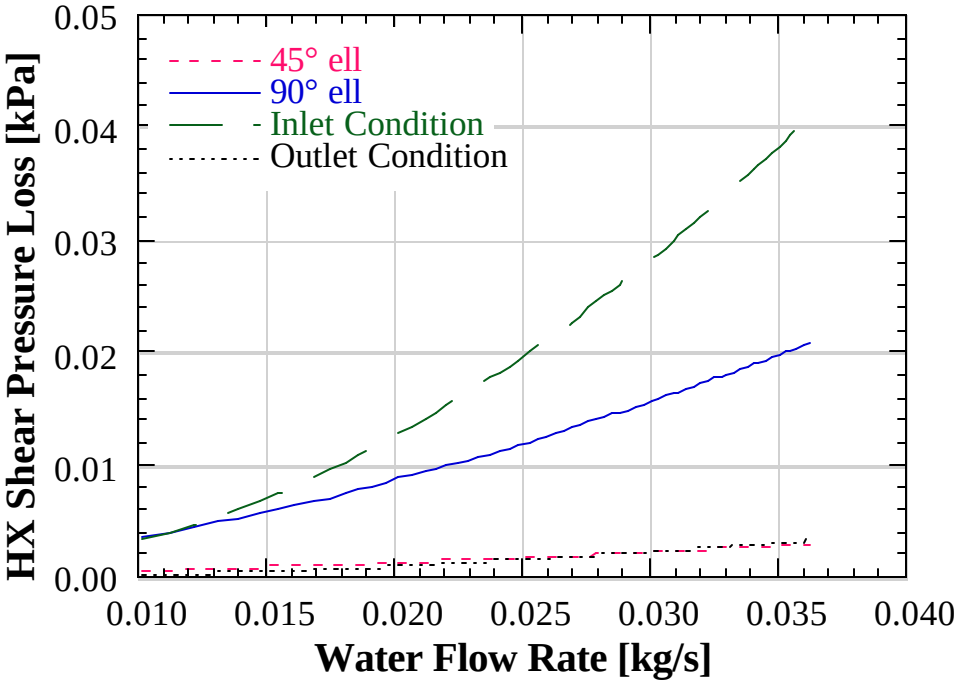

Figure 4.2.6 Comparison of minor loss shear pressure drops.

Figure 4.2.6 compares the NCHE minor loss shear pressure drops for the four minor loss conditions. The pipe inlet condition yielded the greatest pressure loss, followed by the 90° ell. The other two minor loss conditions were found to be much smaller. The pressure loss due to the heat exchanger walls was found to be negligible. Figure 4.2.7 compares the total NCHE shear pressure drop due to minor losses using table values versus using Hooper's correlation. Although the difference between the two curves is small, the use of Hooper's correlation, as will be shown, is essential for the success of the model.

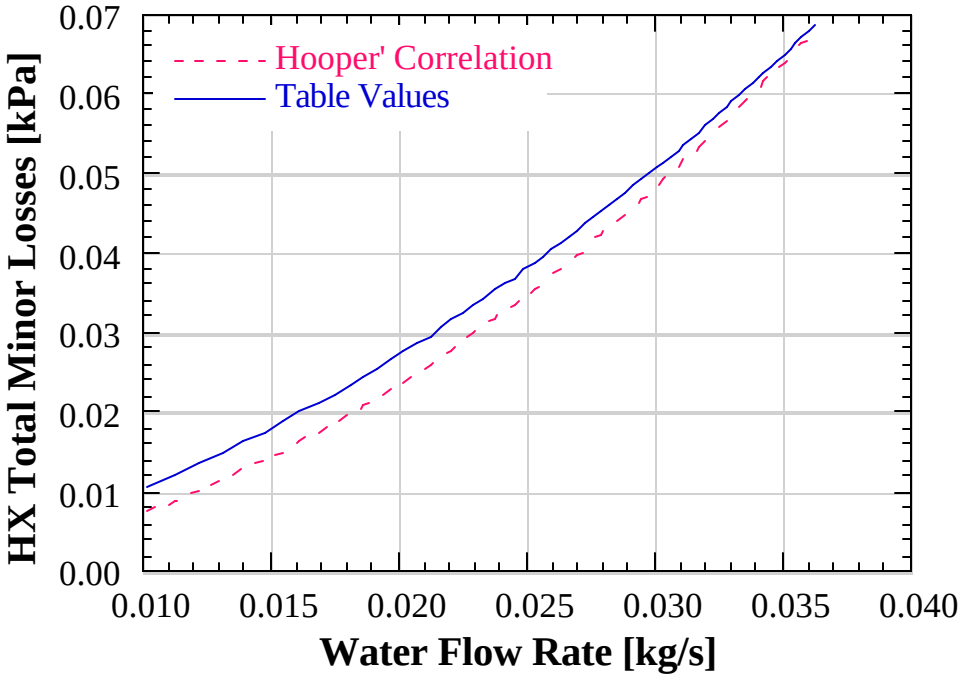

Figure 4.2.7 Comparison of table values and Hooper's correlation (Kakic 1987) for NCHE minor shear pressure losses.

4.2.2 Jakob Pressure Drop Analysis

Jakob presents a simple analysis for the shear pressure drop of a fluid as it moves through a bank of tubes (Chapman 1987). The pressure drop is found by:

$$DP_{sh} = -f_j N\left(\frac{1}{2} r_{w,i} U_{\max}^2\right)\cdot\left(\frac{m_s}{m_{w,i}}\right)^{0.14} \qquad (4.2.1)$$

where Jakob's friction factor is found using:

$$f_j = \left[C_1 + \frac{C_2}{\left(\frac{S_T}{D} - 1\right)^n}\right]\cdot \mathrm{Re}_{D,\max}^{-m} \qquad (4.2.2)$$

and where:

$\rho_{w,i}$ = water density at HX inlet ,

U_{max} = maximum water velocity in HX ,

μ_s = viscosity at average tube surface temperature ,

$\mu_{w,i}$ = water viscosity at HX inlet ,

and C_1, C_2, m, n = correlation parameters listed in Table 4.2.2.

Properties are evaluated at the average water temperature, except for $\mu_{w,i}$ and $\rho_{w,i}$, which are evaluated at the water inlet temperature, and μ_s, which is evaluated at the average tube surface temperature. Jakob's pressure drop correlation requires a Reynolds number, $Re_{D,max}$, which is based upon the maximum fluid velocity, U_{max} (which occurs in the transverse flow area), and the diameter of the tubes in crossflow, $D_{t,o}$. The kinematic viscosity, ν, is evaluated at the average heat exchanger water temperature.

$$Re_{D,max} = \frac{U_{max} D_{t,o}}{\nu} \qquad (4.2.3)$$

For an in line tube bundle, Jakob provides the following parameters:

Table 4.2.2 Jakob's Correlation: Parameters for In-Line Tube Bundle

C1	**C2**	**n**	**m**
0.176	0.34 S_L/D	0.43 + 1.13 D/S_T	0.15

4.2.3 Yawed Tube Correction Factor

Work has been done on a correction factor that allows crossflow correlations to work for tube bundles at angles other than perpendicular to the external flow. Figure 4.2.8 presents a graph of the yaw angle correction factor, C_b, as a function of yaw angle, b (Kakic 1987). To simplify the analysis a function was written for the yaw angle correction factor:

$$C_b = -1.976 + 0.12699b - 2.498\times10^{-3}b^2 + 2.476\times10^{-5}b^3 - 9.5571\times10^{-8}b^4 \qquad (4.2.4)$$

An average yaw angle was found for the heat exchanger under study to be 80.1°, which corresponds to a correction factor of 0.96. This pressure drop equation was multiplied by the yaw correction factor.

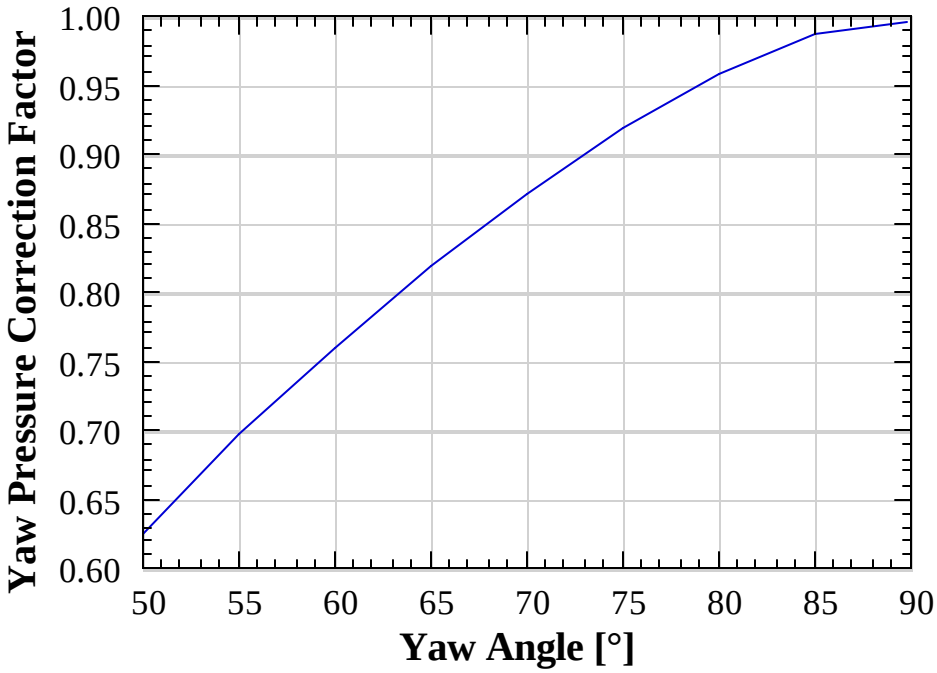

Figure 4.2.8 Yaw angle pressure drop correction factor.

4.2.4 Comparison of Detailed Pressure Drop Model to Experimental Curves

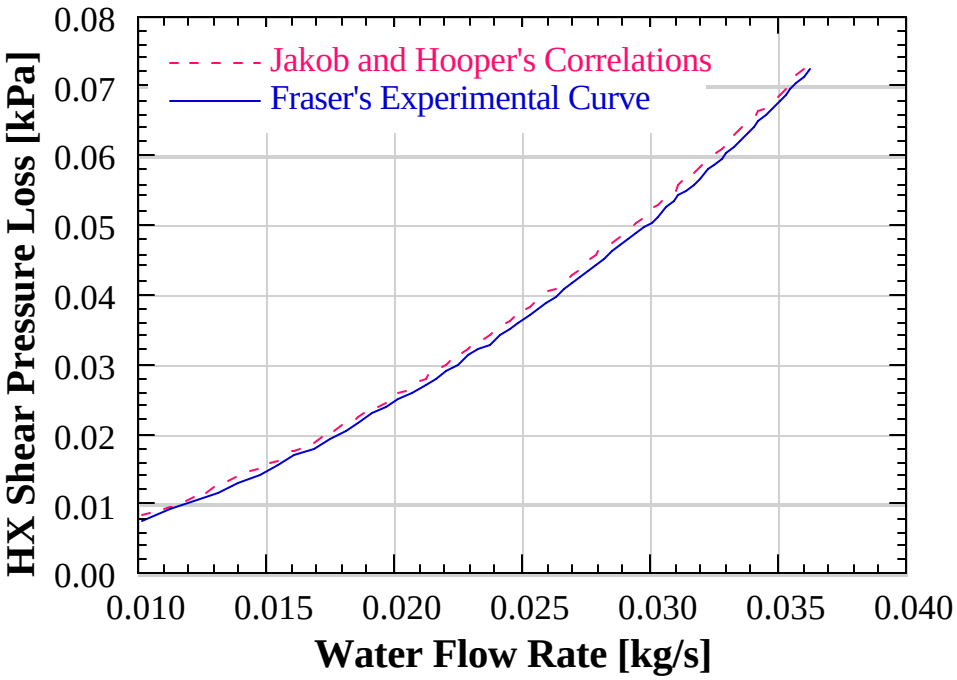

Figure 4.2.9 Comparison of detailed model's NCHE shear pressure loss to Fraser's experimental curve.

Figure 4.2.9 presents a comparison of the detailed model to Fraser's experimental curves. The Jakob analysis resulted in percentage errors averaging 3.3% over the range shown.

In Figure 4.2.10 the total NCHE pressure loss was found using Jakob's correlation, both with and without the yaw angle correction factor, the properties correction term, and the use of Hooper's minor loss coefficient correlation. It was discovered that both the properties and yaw angle correction factors had negligible influence on the result, whereas the use of Hooper's correlation had a major effect on the analysis.

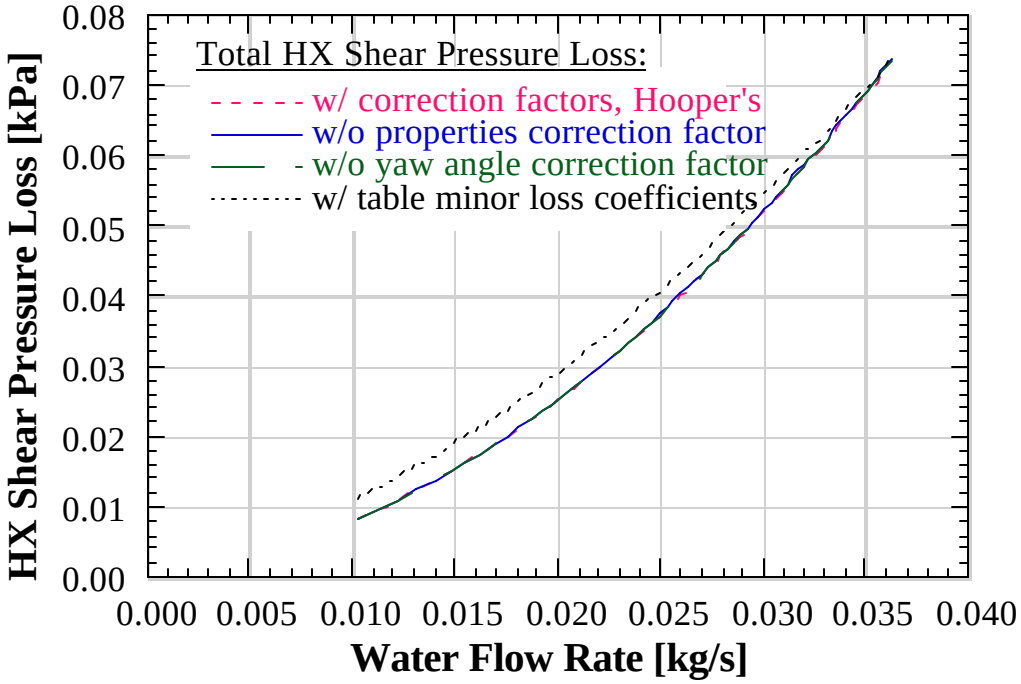

Figure 4.2.10 Effect of correction terms and Hooper's correlation on accuracy of model.

4.3 Detailed Model Heat Transfer Analysis

Several methods were used to calculate the heat transfer of the NCHE. All methods gave approximately the same results. Correction factors were applied for yaw angles and variable properties, but these had virtually no effect on the heat transfer. The heat transfer was found by dividing the NCHE into nodes, determining temperature distributions, and integrating the flux. The heat transfer was also found by treating the NCHE as one section and taking an average temperature at which to find the properties. Both approaches yielded the similar results. The one section method was used, and is described below.

In the NCHE, there will be both forced convection due to pressure differences around the loop, and natural convection within the heat exchanger itself. Fraser developed a density correction factor to account for the natural convection in a specific heat exchanger for low water flow rates. However this density correction factor cannot be applied to other shell and coil heat exchangers, and is consequently of no use for the detailed model.

In order to analyze the heat transfer of the shell and coil heat exchanger, two convection heat transfer coefficients need to be determined: one for the inside of the helical tubes, and one for flow over the outside of the helices. The internal heat transfer coefficients are determined using correlations for flow insides helices and straight tubes, while the external heat transfer coefficients are determined using correlations for flow over bundles of straight tubes in crossflow. A recent correlation for natural convection from enclosed vertical helical tubes is also considered.

4.3.1 The Modified Effectiveness-NTU Approach

The modified effectiveness-NTU approach is used in determining the heat transfer. The UA_s value of the heat exchanger is found using:

$$UA_s = \frac{1}{\frac{1}{h_i A_{s,i}} + \frac{1}{h_o A_{s,o}}} \tag{4.3.1}$$

where $A_{s,o}$, $A_{s,i}$, h_o, and h_i, are the outer and inner tube surface areas and the outer and inner heat transfer coefficients respectively. The resistance of the copper wall is assumed to be negligible. The modified number of transfer units is found using:

$$NTU = \frac{UA_s}{\left(\dot{m}C_p\right)_g} \tag{4.3.2}$$

The modified effectiveness can then be found using the relationships presented in Sections 3.3.2-3.

4.3.2 Zukauskas' Correlation for Tube Bundles in Crossflow

No heat transfer correlations could be found for the heat transfer associated with *forced* flow over helical tubes. Consequently Zukauskas' heat transfer correlation for tube bundles in crossflow was used. Zukauskas' correlation has a 15% uncertainty. More inaccuracy may result from this particular analysis, as flow over the helical coils will be of a similar, but different nature than flow over tubes in crossflow. The flow over the helical coils may produce a swirling motion that tubes in crossflow would not. The swirling motion increases the movement of the water, thereby enhancing heat transfer. As the model does not account for this, the detailed model should underpredict the heat transfer.

As described in Section 4.1, the helical tubes were reduced to an array of tubes in crossflow. An average heat transfer coefficient for a bank of tubes is found using Zukauskas' correlation:

$$\overline{Nu}_o = C\,\mathrm{Re}_{D,\max}^{m}\,\mathrm{Pr}^{n}\left(\frac{\mathrm{Pr}}{\mathrm{Pr}_s}\right)^{1/4} \qquad (4.3.3)$$

where Pr was evaluated at the average heat exchanger water temperature, Pr_s, at the average tube surface temperature and where the constants C, m and n, varied depending upon the Reynolds number as is shown in Table 4.3.1. Like Jakob's correlation, Zukauskas' crossflow correlation requires a Reynolds number, $\mathrm{Re}_{D,\max}$, which is based upon the maximum fluid velocity, $U_{\max}$, and the diameter of the tubes in crossflow, $D_{t,o}$. The kinematic viscosity, u, is evaluated at the average heat exchanger water temperature.

$$\mathrm{Re}_{D,\max} = \frac{U_{\max} D_{t,o}}{u} \qquad (4.3.4)$$

Table 4.3.1 Zukaukas' Correlation Parameters

$\mathbf{Re_{D,max}}$	**C**	**m**	**n**
0 - 100	0.9	0.4	0.36
100 - 1000	0.52	0.5	0.36

Reynolds numbers range in this analysis from 0 to 150. Calculations made using both sets of parameters in Table 4.3.1 gave essentially the same results. Either set of parameters thus is sufficient. The coefficients applying to the lower range of Reynolds numbers are used.

As the Zukauskas crossflow heat transfer correlation assumes constant temperature tubes, (which is not the case here), an average tube temperature must be found in order to use the correlation to find the Nusselt number. The resistance of the tube wall is assumed to be negligible, hence the inner and outer surfaces are assumed to be at the same temperature. The average tube temperature was found using:

$$Q_{HX} = h_i A_{s,i} (\overline{T}_s - \overline{T}_w) \qquad (4.3.5)$$

where $A_{s,i}$ = inner tube surface area
$\overline{T}_s$ = tube surface temperature
$\overline{T}_w$ = average HX water temperature

4.3.3 Allen and Ajele's Correlation for Natural Convection Heat Transfer from Enclosed Helical Coils in a Vertical Orientation

Zukauskas' crossflow correlation relies primarily upon the Reynolds number of the water flow in an equivalent crossflow heat exchanger. Another method of determining the water-side heat transfer coefficient relies solely upon water properties in the heat exchanger. Allen and Ajele (1994) have presented correlations for natural convection heat transfer from enclosed helical coils in a vertical orientation. Coils ranging in mean diameter from 0.0268 to 0.0887 m were tested in 6 combinations of 2, 3 and 4 coils enclosed in a constant diameter shell of 0.1 m.

According to Allen and Ajele, rather than the tube or coil diameter, the geometric factor of most significant influence on the thermal performance of a shell and coil heat exchanger may be the dimensionless flow space, S'. The dimensionless flow space is defined as the ratio of the equivalent total flow space to an equivalent diameter of the coils. The equivalent diameter, D_{eq}, is the diameter one would find if the cross sectional areas taken up by the coils were combined into an equivalent circle. The equivalent diameter is found using:

$$D_{eq}^2 = \sum_{j=1}^{N} \left(D_{cj,o}^2 - D_{cj,i}^2 \right) \qquad (4.3.6)$$

where N is the number of coils and $D_{c,o}$ and $D_{c,i}$ are the coil inner and outer diameters respectively.

The dimensionless flow space, S', is defined as:

$$S' = \frac{\left(D_{shell} - D_{eq} \right)}{D_{eq}} \qquad (4.3.7)$$

where D_{shell} is the shell diameter.

The hydraulic diameter was found using:

$$D_{hx} = \frac{4\,A_{cf}\,H}{A_p} \tag{4.3.8}$$

where A_p is the surface area equivalent of the wetted perimeter, and is given as the sum of the total heat transfer area of the tube outer surface and the shell inner surface.

$$A_p = A_{o,t} + A_s = \pi\ D_{o,t}\ L_t + \pi\ D_s\ H \tag{4.3.9}$$

The flow cross-sectional area on the water-side of the heat exchanger, A_{cf}, is given by:

$$A_{cf} = \frac{\pi\left(D_s^2 - D_{eq}^2\right)}{4} \tag{4.3.10}$$

Dimensionless parameters that are based upon a characteristic length are based upon the hydraulic diameter in this analysis. The Rayleigh number is defined as

$$Ra_{Dhx} = \frac{\beta\, g\left(\overline{T}_s - T_\infty\right)D_{hx}^3}{\upsilon\alpha} \tag{4.3.11}$$

where T_∞ is the inlet temperature of the water far from the heat exchanger inlet (T_∞ is taken as $T_{w,i}$). To obtain Rayleigh numbers that are representative of the buoyancy induced flow in the heat exchanger, Ra_{Dhx} was modified by the ratio of the heat exchanger height to total length of tubing. The modified Rayleigh number and Nusselt numbers are given by:

$$Ra^*_{Dhx} = \frac{Ra_{Dhx}\,H}{L_t} \tag{4.3.12}$$

$$Nu_{Dhx} = \frac{h_o\,D_{hx}}{k} \tag{4.3.13}$$

The flow number, which represents the energy available in the hot stream relative to the ability of the cold stream to absorb it (Richmond and Hollands 1987) is given by:

$$F = \frac{\left(\dot{m} C_p\right)_g D_t}{2 k_g A} \tag{4.3.14}$$

where D_t is the mean diameter of the tube and A is the total surface area based on D_t.

Allen and Ajele present the following correlations for natural convection flow over enclosed helices.

$$Nu_{Dhx} = 0.563 S'^{m} \left(F^{\left\lceil (N_c - 1)/3 \right\rceil} Ra^* \right)^{0.323} \tag{4.3.15}$$
$$F < 1, \quad 10^3 < Ra^* < 2 \times 10^5$$

$$Nu_{Dhx} = 0.552 \left(Ra^* \right)^{0.322} \tag{4.3.16}$$
$$F > 1, \quad 2 \times 10^3 < Ra^* < 2 \times 10^6$$

where N_C is the number of coils. The values of m depend upon N_C, and are presented in Table 4.3.2.

Table 4.3.2. Exponent m Values for Use in Allen and Ajele's Correlation for 2, 3 or 4 Coils

N_C	2	3	4
m	-1/3	1/5	0

Figure 4.3.1 presents a steady state comparison of heat transfer coefficients found using Allen and Ajele's correlation and Zukaukas' crossflow correlation. The two correlations yield widely differing heat transfer coefficients.

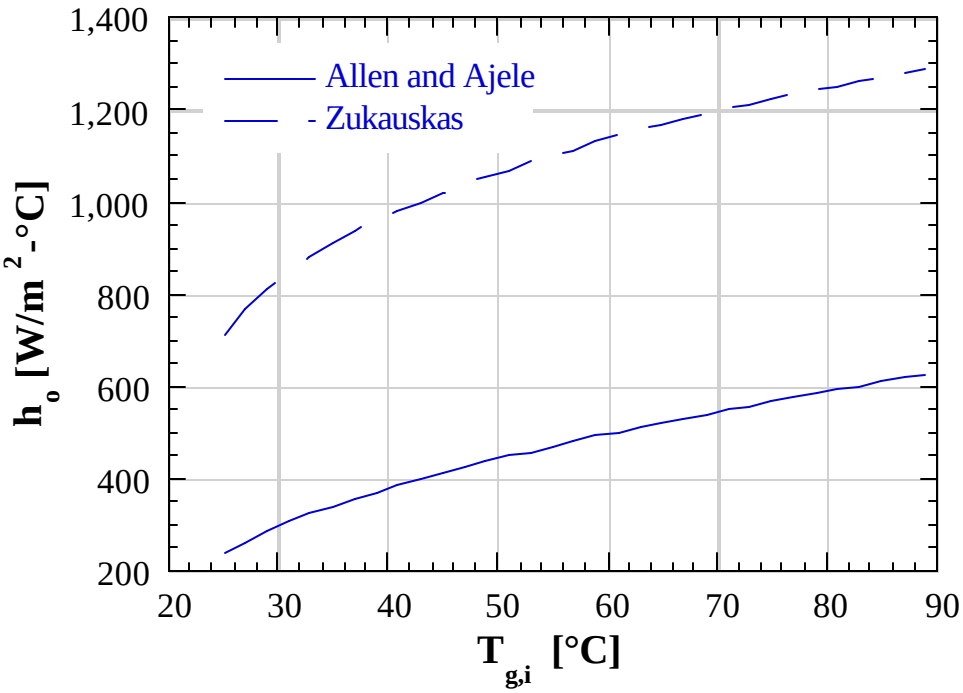

Figure 4.3.1 Steady state comparison of Allen and Ajele's and Zukauskas' correlations: h_o as a function of $T_{g,i}$.

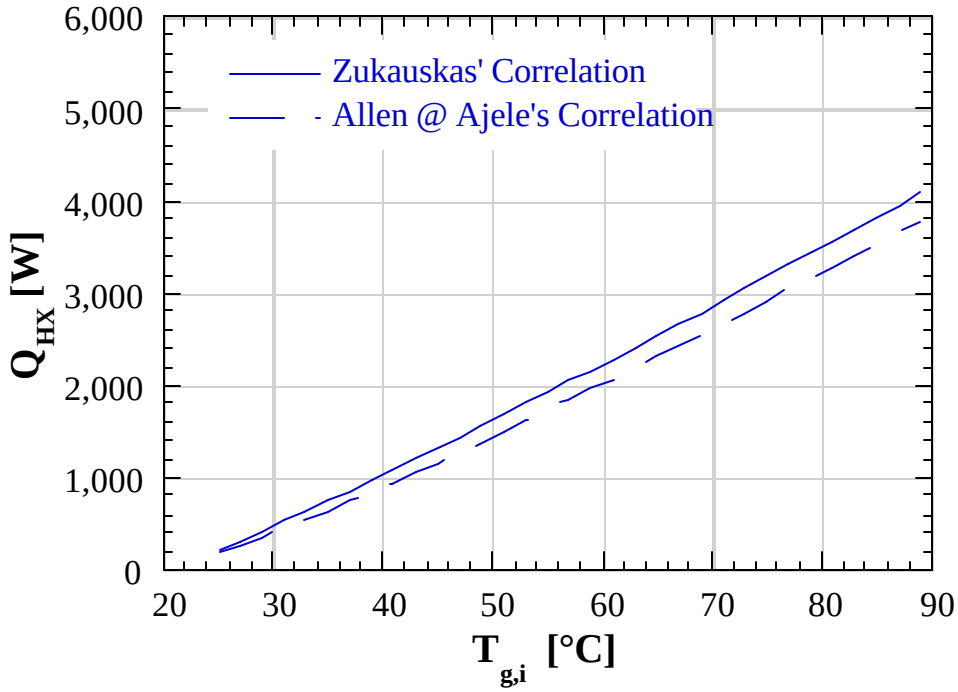

Figure 4.3.2 Steady state comparison of Allen and Ajele's and Zukauskas' correlations: Q as a function of $T_{g,i}$.

Although the two water-side correlations provide vastly different Nusselt numbers, the heat transfer rate using the two correlations is nearly the same, with percent differences averaging about 8%, as is shown in Figure 4.3.2. That the heat transfer rates in Figure 4.3.2 agree so well, in spite of such different heat transfer coefficients, can be attributed to the "long" nature of the heat exchanger. A representative temperature distribution is presented in Figure 4.3.3. As the change in glycol temperaure is much greater than the change in water temperature, the glycol capacitance rate is the limiting capacitance rate. As a result, changes in the water-side heat transfer coefficient lead to very small changes in heat transfer rate, as the heat transfer on the glycol side is the limiting factor.

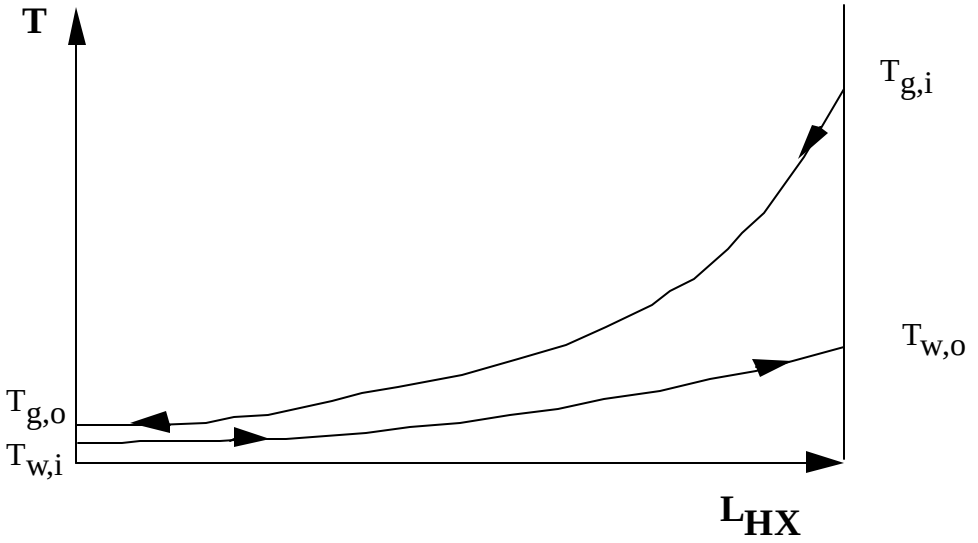

Figure 4.3.3 Temperature distribution for heat exchanger. Notice how the glycol outlet temperature approaches the water inlet temperature. As the glycol capacitance rate is the limiting factor in this heat exchanger, changes in the water-side heat transfer coefficient have little effect upon the heat transfer rate.

For the heat exchanger under study, enclosed helical coils in a vertical orientation, it is preferable to use correlations found explicitly for that geometry. That is, it is preferable to apply Allen and Ajele's correlations for flow over helices, than Zukauskas' correlations for crossflow over tube bundles. However, there are some restrictions in Allen and Ajele's analysis that prevent their correlation from

being useful in the detailed model. Allen and Ajele tested the coil combinations in a constant diameter shell. As is shown in Figure 4.3.4, for some combinations of coils, as there is significant flow area between the outermost coil and the heat exchanger shell, in forced flow conditions much of the water flow can bypass the coils, thereby reducing the heat transfer in the heat exchanger. In contrast, the heat exchanger designs considered in the detailed model consider heat exchanger shell diameters that are sized slightly larger than the largest coils' outer diameter. Also, Allen and Ajele's correlation is applicable to combinations of 2, 3 or 4 coils only, whereas the crossflow correlations are applicable for 2 or more coils.

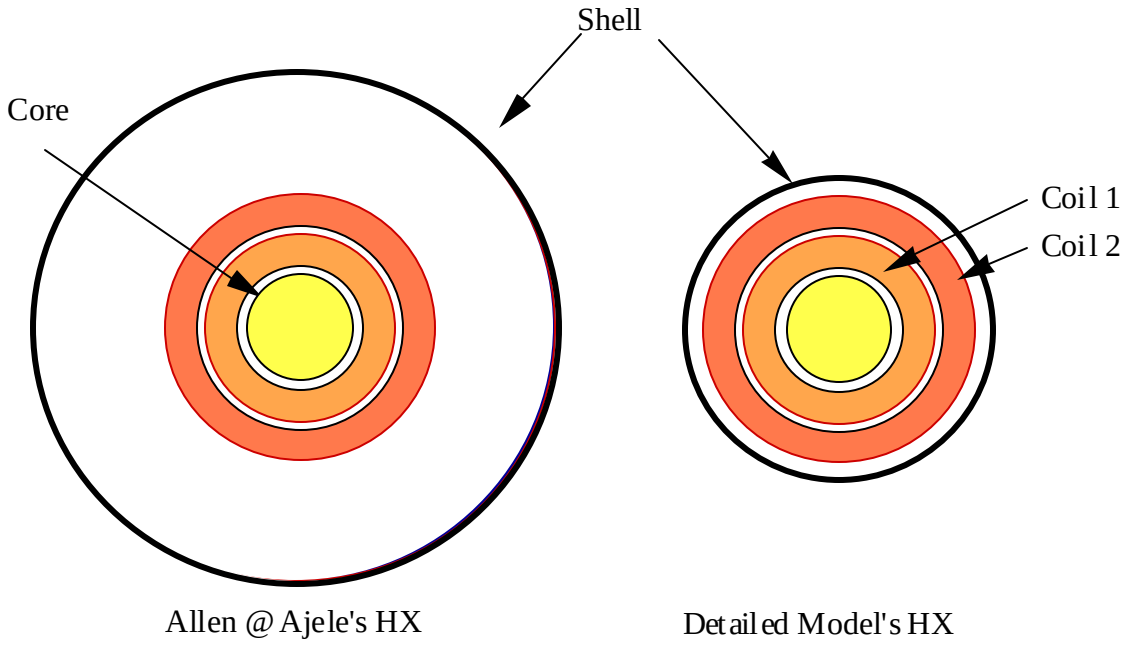

Figure 4.3.4 On the left, top cut-away view of Allen and Ajele's experimental heat exchanger for combination of coils 1 and 2. Note the significant flow area between the outermost coil and the shell. On the right, the detailed model's heat exchanger employing the same coil combination.

In summary, as both Allen and Ajele's and Zukauskas' correlations provide nearly the same heat transfer rates, either correlation could be used to find the water-side Nusselt number. Although Allen and Ajele's analysis is geometrically more appropriate than crossflow analysis, limitations

described above limit the applicability of Allen and Ajele's correlation for use in the detailed model. Consequently, Zukauskas' crossflow correlation is used in the detailed model.

4.3.4 Manlapanz and Churchill's Correlation for Internal Flow Inside Helical Tubes

Heat transfer is greater in helical tubes than in straight tubes due to the secondary flows that are established in the tubes. Flow tends to be more irregular, with higher fluid velocities at the outer tube wall and lower fluid velocities at the inner wall. The higher fluid velocities considerably decrease thermal resistance in the fluid, thereby yielding greater heat transfer coefficients in helical tubes. Manlapanz and Churchill's correlation (Kakic 1987) for flow in helical tubes was used to find the Nusselt number for the glycol flow, in which constant heat flux was assumed.

$$Nu_i = \left[\left(4.364 + \frac{4.636}{x_1} \right)^3 + 1.816 \left(\frac{De}{x_2} \right)^{3/2} \right]^{1/3} \tag{4.3.17}$$

where:

$$x_1 = \left(1 + \frac{1352}{De^2 \, \mathrm{Pr}} \right)^2 \tag{4.3.18}$$

and:

$$x_2 = 1 + \frac{1.15}{\mathrm{Pr}} \tag{4.3.19}$$

The Dean number, a non-dimensionalized parameter which accounts for secondary flow in the helix, is found using:

$$De = \mathrm{Re} \sqrt{\frac{a}{R}} \tag{4.3.20}$$

where a represents the tube radius, and R represents the radius of curvature of the helix.

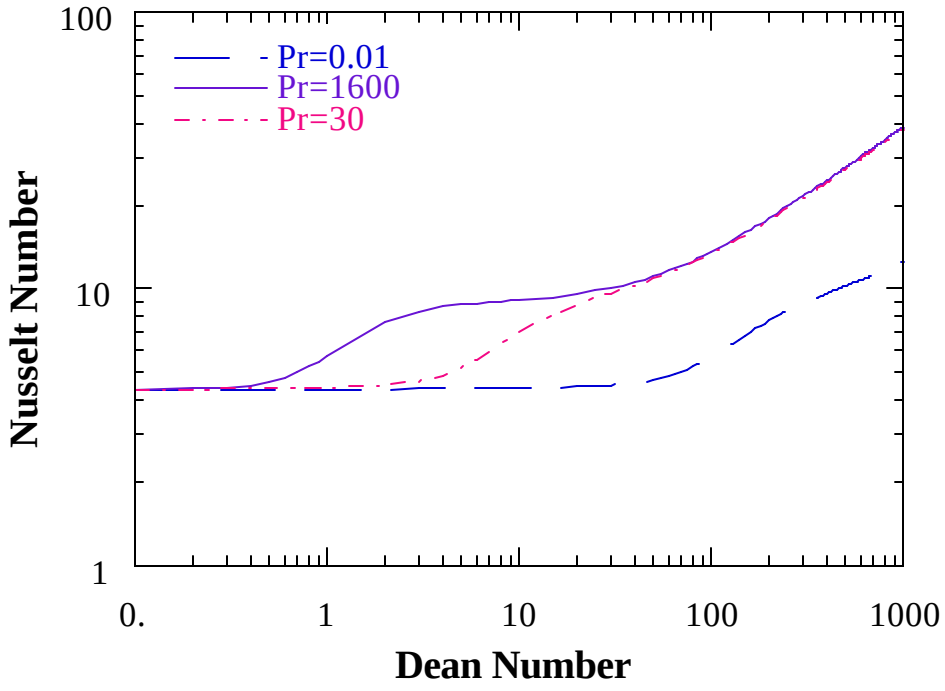

Figure 4.3.5 Manlapanz and Churchill's correlation for flow in helices (Kakic 1987).

As the radius of curvature approaches infinity (as it does for straight tubes), the Nusselt number approaches 4.364, which is the Nusselt number for laminar, constant flux flow in straight tubes as is shown in Figure 4.3.5.

Rather than find a Nusselt number for each coil in the NCHE, an average length and diameter coil was used. The glycol flow rate used in the analysis then is one-fourth the true glycol flow rate, as there were 4 coils.

Figures 4.3.6-7 compare the heat transfer and consequent water flow rate of the detailed model employing the Manalpanz and Churchill correlation against the simple model. For glycol temperatures below 80°C, the detailed model predicts a heat transfer rate that is 15% more than the simple model's prediction.

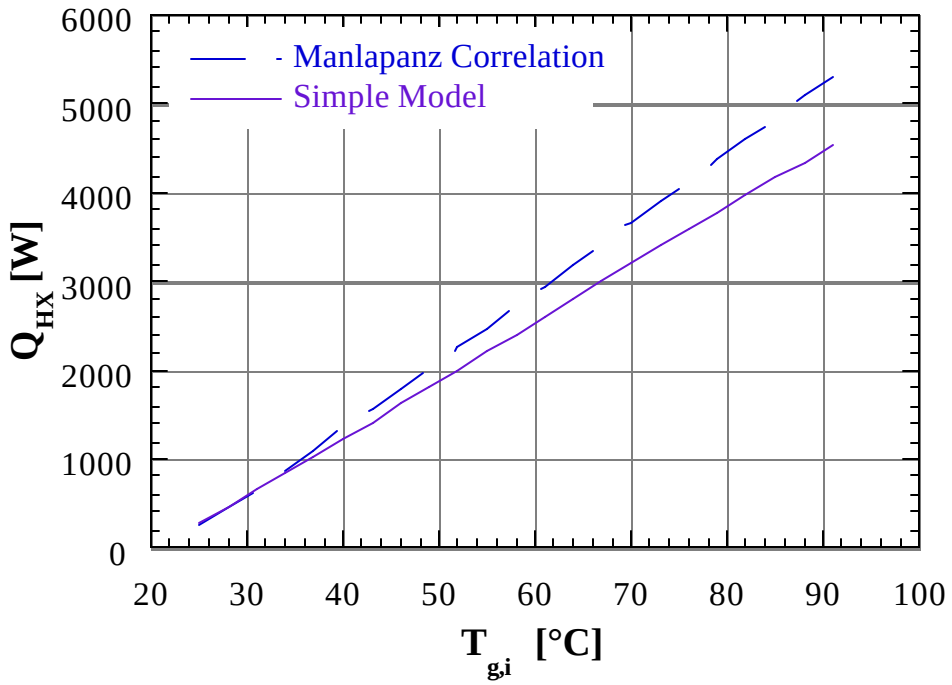

Figure 4.3.6 Comparison of heat transfer rate for simple model and detailed model employing Manlapanz and Churchill's correlation for flow in helices.

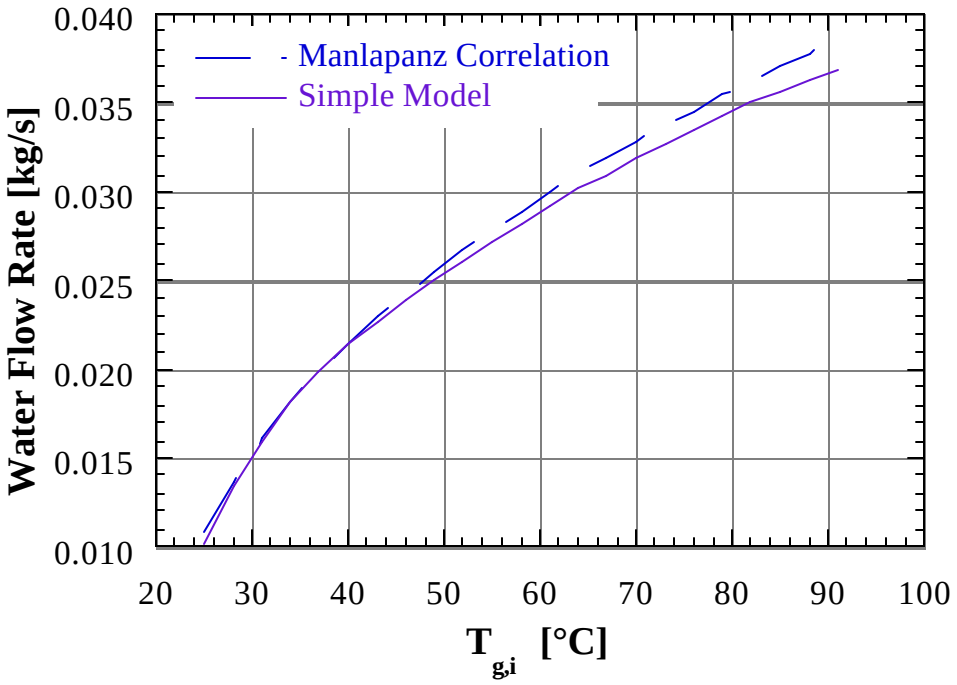

Figure 4.3.7 Comparison of water flow rate for simple model and detailed model employing Manlapanz and Churchill's correlation for flow in helices.

Although Zukauskas predicted 15% uncertainty for his correlation, and simulation results fall within that 15% for most of the range presented, another correlation inserted in place of the Manlapanz correlation might offer more accurate results.

4.3.5 Correlation for Internal Flow for Straight Tubes

A Nusselt number relation for fully developed, laminar flow in a straight tube was used in place of Manlapanz and Churchill's helical tube correlation, namely,

$$Nu_o = 4.36 \qquad (4.3.21)$$

As heat transfer is greater in helical tubes than in straight tubes due to secondary flows within the helices, this correlation should underpredict the inside heat transfer coefficient, h_i, which, in turn, should lead to a low estimate for the heat transfer.

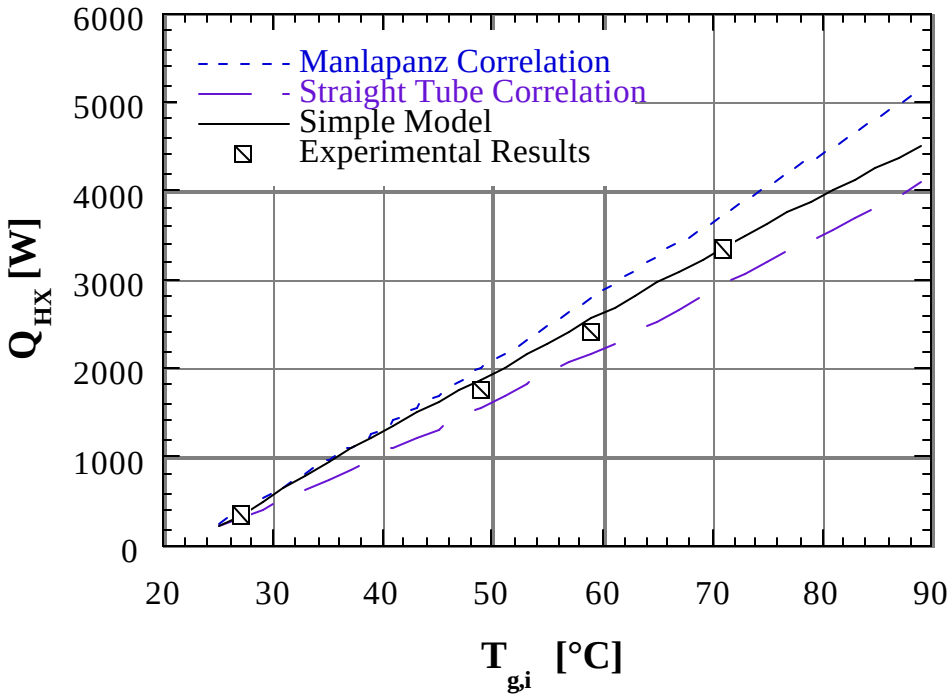

Figure 4.3.8 Comparison of the detailed model and the simple model in finding heat flux.

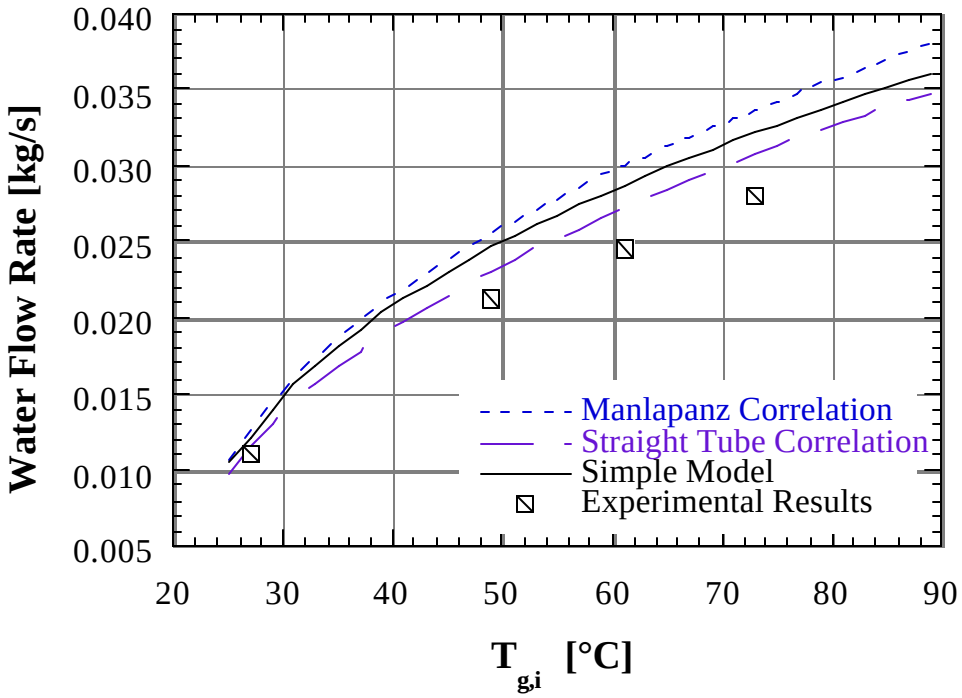

Figure 4.3.9 Water flow rate: a comparison of the detailed models to the simple model.

Figures 4.3.8 and 4.3.9 compare the use of the two correlations on the heat transfer and the water flow rate of the heat exchanger. The Manlapanz correlation produces better values of the heat transfer below 55°C, while the straight tube correlation yields better values for glycol inlet temperatures above 55°C.

4.4 Transient Comparison of Detailed Model to Simple Model

From the data presented in Figure 4.3.8-9, it is difficult to decide which glycol-side correlation better predicts the heat transfer in the heat exchanger. Consequently, yearly transient simulations were executed for Madison employing both of the glycol-side correlations. Both correlations performed remarkably well. Figure 4.4.1 compares the monthly solar fraction for the detailed model, employing each of the two correlations, to the simple model; while Table 4.4.1 compares the

yearly solar fraction and total auxiliary energy required. The use of the Manlapanz correlation overestimates the solar fraction, while the use of the straight tube correlation underestimates the solar fraction.

Table 4.4.1 Comparison of Detailed and Simple Models for a One-Year Simulation.

Model	Q_{aux} [MJ]	Solar Fraction
Simple	9986.3	0.5111
Detailed - Manlapanz	9794.5	0.5204
Detailed - Straight Tube	10309.3	0.4953
% Error - Manlapanz	1.92	1.84
% Error - Straight Tube	3.23	3.08

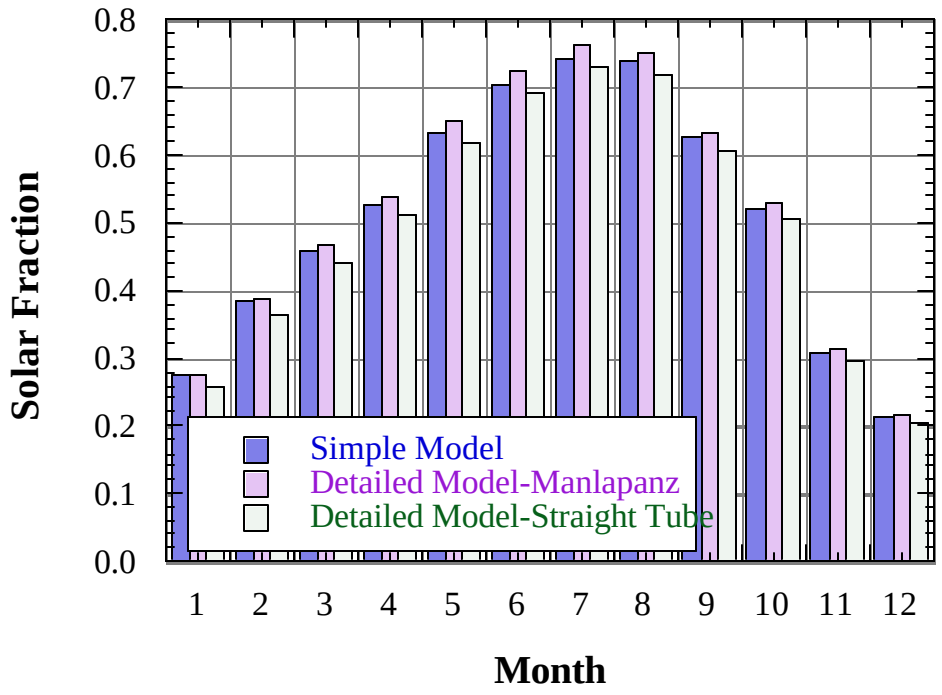

Figure 4.4.1 Comparison of monthly solar fraction for the detailed and simple models.

As the Manlapanz correlation provides solar fraction values closer to those of the simple model, the Manlapanz correlation has been chosen for inclusion in the detailed model.

A conservative assumptions was made in the writing of the detailed model:

1) by using Zukauskas' crossflow correlation, the enhanced heat transfer due to the swirling motion of water over helical coils was neglected.

This conservative assumption should lead to an underprediction of the heat transfer in the heat exchanger. When a second conservative assumption is made,

2) the helical tubes can be considered to be straight, and consequently the straight tube correlation can be utilized in place of the Manlapanz helical tube correlation,

the heat transfer is underpredicted as expected. However, contrary to expectations, when the Manlapanz correlation is employed, the heat transfer is overpredicted. No cogent explanation can be offered for the over predictions in the simulation, but instead a reminder that Zukauskas' crossflow correlation is only accurate to 15%.